Halo nuclei ^{6}He and ^{8}He with the Coulomb-Sturmian basis

M. A. Caprio, P. Maris, and J. P. Vary

Halo nuclei ^{6}He and ^{8}He with the Coulomb-Sturmian basis

M. A. Caprio

Department of Physics, University of Notre Dame,

Notre Dame, Indiana 46556-5670, USA

P. Maris and J. P. Vary

Department of Physics and Astronomy,

Iowa State University, Ames, Iowa 50011-3160, USA

The rapid Gaussian falloff of the oscillator functions at large radius makes them poorly suited for the description of the asymptotic properties of the nuclear wave function, a problem which becomes particularly acute for halo nuclei. We consider an alternative basis for *ab initio* no-core configuration interaction (NCCI) calculations, built from Coulomb-Sturmian radial functions, allowing for realistic exponential falloff. NCCI calculations are carried out for the neutron halo nuclei ^{6,8}He, as well as the baseline case ^{4}He, with the JISP16 nucleon-nucleon interaction. Estimates are made for the root-mean-square radii of the proton and matter distributions.

I. INTRODUCTION

The *ab initio* theoretical description of light nuclei is based on direct solution of the nuclear many-body problem given realistic nucleon-nucleon interactions. In no-core configuration interaction (NCCI) calculations [1–3], the nuclear many-body problem is formulated as a matrix eigenproblem. The Hamiltonian is represented in terms of basis states which are antisymmetrized products of single-particle states for the full A-body system of nucleons, *i.e.*, with no assumption of an inert core.

In practice, the nuclear many-body calculation must be carried out in a truncated space. The dimension of the problem grows combinatorially with the size of the included single-particle space and with the number of nucleons in the system. Computational restrictions therefore limit the extent to which converged results can be obtained, for energies or for

other properties of the wave functions. Except for the very lightest systems ($A \lesssim 4$), convergence is generally beyond reach. Based on the still-unconverged calculations which are computationally feasible, we seek to obtain a reliable estimate of the true values of observables which would be obtained in the full, untruncated space. Improved accuracy may be pursued both through the development of bases which yield accelerated convergence, as considered here, and by developing means by which robust extrapolations can be made [4–10].

A prominent feature in light nuclei is the emergence of halo structure [11, 12], in which one or more loosely-bound nucleons surround a compact core, spending much of their time in the classically-forbidden region. A realistic treatment of the long-range properties of the wave function has been found to be essential for an accurate reproduction of the halo structure [13].

However, NCCI calculations have so far been based almost exclusively upon bases constructed from harmonic oscillator single-particle wave functions. The harmonic oscillator radial functions have the significant limitation that they display Gaussian asymptotic behavior, *i.e.*, falling as $e^{-\alpha r^2}$ for large r. The actual asymptotics for nucleons bound by a finite-range force are instead expected to be exponential, *i.e.*, falling as $e^{-\beta r}$.

Observables which are sensitive to the large-distance asymptotic portions of the nuclear wave function present a special challenge to convergence in NCCI calculations with a conventional oscillator basis. Such "long-range" observables include the root-mean-square (RMS) radius — an essential observable for halo nuclei — and $E2$ moments and transitions. The r^2 dependence of the relevant operators in both cases preferentially weights the larger-r portions of the wave function. The results for these observables in NCCI calculations are in general highly basis-dependent [5, 14, 15].

The difficulties encountered in using an oscillator basis to describe a system with exponential asymptotics may be illustrated through the simple one-dimensional example of the Schrödinger equation with a Woods-Saxon potential. In Fig. 1, we see the results of solving for a particular eigenfunction in terms of successively larger bases of oscillator radial functions. In the classically forbidden region, where the potential is nearly flat, the tail of the wave function should be exponential. It should thus appear as a straight line on the logarithmic scale in Fig. 1. Inclusion of each additional basis function yields a small extension to the region in which the expected straight-line behavior is reproduced. However, for
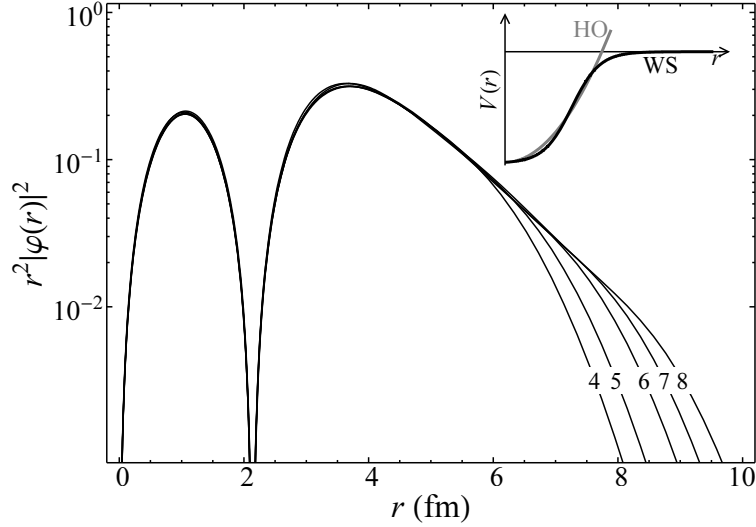
FIG. 1: The calculated wavefunction obtained when a problem with exponential asymptotics — here, the Woods-Saxon problem is taken for illustration — is solved in a finite basis of oscillator functions. The radial probability density $r^2|\varphi(r)|^2$ is shown on a logarithmic scale, so that exponential asymptotics would appear as a straight line. The Woods-Saxon (WS) and harmonic oscillator (HO) potentials are shown in the inset. (Solutions are for the Woods-Saxon $1s_{1/2}$ function, with potential parameters appropriate to neutrons in ^{16}O [16], with maximal basis radial quantum numbers n as indicated.)

any finite number of oscillator functions, there is a radius beyond which the calculated tail is seen to sharply fall below the true asymptotics.

We are therefore motivated to consider alternative bases which might be better suited for expanding the nuclear wave function in its asymptotic region. The Coulomb-Sturmian functions [17], which are obtained as solutions of the Sturm-Liouville problem associated with the Coulomb potential, constitute a complete set of square-integrable functions with exponential asymptotics. These functions have previously been applied to few-body problems in atomic [18–20], hadronic [21–23], and nuclear [24] physics. The framework for carrying out NCCI calculations with general radial basis functions — and with the Coulomb-Sturmian functions, in particular — has been developed in Ref. [25].

In the present work, we apply the Colomb-Sturmian basis to NCCI calculations for the lightest neutron halo nuclei — ^{6,8}He — as well as to the baseline case ^{4}He, for which converged results can be obtained. Motivated by the disparity between proton and neutron

radial distributions in the neutron-rich halo nuclei, we explore the use of proton-neutron asymmetric bases, with different length scales for the proton and neutron radial basis functions. We also examine the possibility of extracting RMS radii for the proton and matter distributions based on a relatively straightforward estimate, the "crossover point" [5, 14], pending further development of more sophisticated extrapolation schemes [26, 27]. The bases and methods are first reviewed (Sec. II), after which the results for ^{4,6,8}He are discussed and compared with experiment (Sec. III). Details of the calculation of RMS radii for general single-particle bases are given in the Appendix. Preliminary results were reported in Ref. [28].

II. BASIS AND METHODS

A. Basis functions

The harmonic oscillator and Coulomb-Sturmian functions both provide complete, discrete, orthogonal sets of square-integrable functions, but with Gaussian and exponential asymptotics, respectively. The oscillator functions [29], as used in conventional NCCI calculations, are given by $\Psi_{nlm}(b; \mathbf{r}) = R_{nl}(b; r)Y_{lm}(\hat{\mathbf{r}})/r$, with radial wave functions

$$R_{nl}(b; r) \propto (r/b)^{l+1}L_n^{l+1/2}[(r/b)^2]e^{-\frac{1}{2}(r/b)^2}, \tag{1}$$

where b is the oscillator length. The Coulomb-Sturmian functions [17] are given similarly by $\Lambda_{nlm}(b; \mathbf{r}) = S_{nl}(b; r)Y_{lm}(\hat{\mathbf{r}})/r$, with radial wave functions

$$S_{nl}(b; r) \propto (2r/b)^{l+1}L_n^{2l+2}(2r/b)e^{-r/b}, \tag{2}$$

where b again represents a length scale. Further discussion may be found in Ref. [25]. In both sets of functions (1) and (2), the L_n^α are generalized Laguerre polynomials, the Y_{lm} are spherical harmonics, n is the radial quantum number, and l and m are the orbital angular momentum and its z-projection. Both sets of radial functions are shown in Fig. 2, for comparison.

For the oscillator functions, the principal quantum number $N \equiv 2n + l$ defines the number of oscillator quanta associated with the function, or the major shell to which it is assigned, when considered in the context of an oscillator Hamiltonian with corresponding length parameter b [16]. While the particular combination of n and l represented by N has no
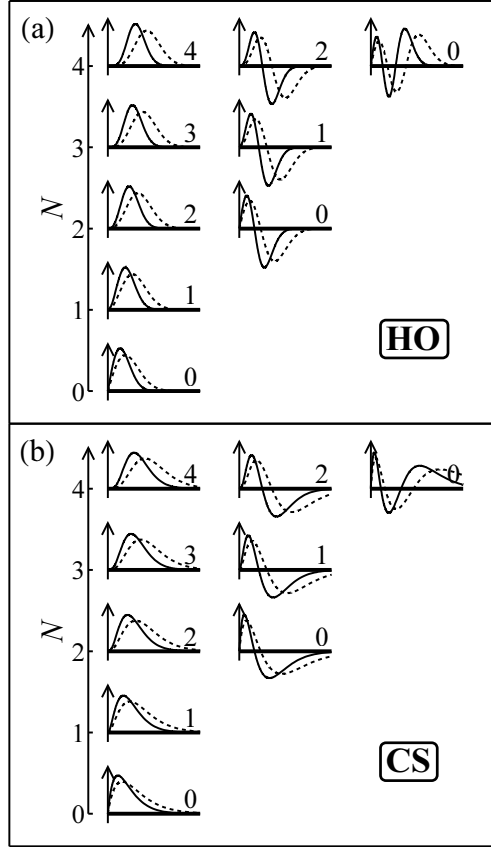
FIG. 2: Radial functions (a) $R_{nl}(b;r)$ of the harmonic oscillator basis and (b) $S_{nl}(b_l;r)$ of the Coulomb-Sturmian basis, with b_l given by the node-matching prescription (6). These functions are shown arranged according to the harmonic oscillator principal quantum number $N \equiv 2n + l$ (see text), and are labeled by l. The dotted curves show the same functions dilated outward by a factor of $\sqrt{2} \approx 1.414$, corresponding to a factor of 2 reduction in $\hbar\Omega$.

immediate physical significance for the Coulomb-Sturmian functions, labeling the Coulomb-Sturmian functions by N, as in Fig. 2(b), can still be of convenience for consistency with the treatment of the oscillator functions.

For either basis, the nuclear single-particle basis states $|nljm\rangle$ are defined by coupling of the orbital angular momentum with the spin, to give total angular momentum j. The many-body basis is defined by taking antisymmetrized products of these single-particle states.

B. Hamiltonian and observables

The structure of the many-body calculation is independent of the details of the radial basis. The choice of radial basis enters the many-body calculation only through the values of the Hamiltonian two-body matrix elements (or higher-body matrix elements, if higher-body interactions are present), which we must first generate as the input to the many-body calculation. The choice of radial basis subsequently also enters into the extraction of observables (electromagnetic moments and transitions, radii, *etc.*), from the densities obtained in the many-body calculation [16]. Here the relevant inputs are the one-body or two-body matrix elements of the observable operators with respect to the given basis.

The nuclear Hamiltonian for NCCI calculations has the form $H = T_{\rm rel} + V$, where $T_{\rm rel}$ is the Galilean-invariant, two-body relative kinetic energy operator, and V is the nucleon-nucleon interaction. A Lawson term [30] proportional to the number $N_{\rm c.m.}$ of center-of-mass oscillator quanta may also be included, to shift center-of-mass excitations out of the low-lying spectrum. (The center-of-mass dynamics for NCCI calculations with the Coulomb-Sturmian basis, including the effect of a Lawson term, are investigated in Ref. [25].) However, a Lawson term is not essential for the present calculations, since we consider only the ground state, and the calculations of observables (discussed below) make use only of relative operators, which are, by construction, insensitive to the center-of-mass degrees of freedom.

The relative kinetic energy decomposes into one-body and two-body terms as

$$
\begin{aligned}
T_{\rm rel} &\equiv \frac{1}{4Am_N} {\sum_{ij}}' (\mathbf{p}_i - \mathbf{p}_j)^2 \\
&= \frac{1}{2Am_N} \left[(A-1) \sum_i \mathbf{p}_i^2 - {\sum_{ij}}' \mathbf{p}_i \cdot \mathbf{p}_j \right],
\end{aligned}
\tag{3}
$$

where the prime on the summation $\sum'_{ij}$ over nucleons indicates $i \neq j$, A is the nuclear mass number, and m_N is the nucleon mass. The one-body term may be calculated simply in terms of one-dimensional radial integrals of the operator p^2, with respect to the radial basis functions. Since the two-body term is separable, matrix elements of this term may likewise be calculated in a straightforward fashion for any radial basis, in terms of radial integrals of the operators p and angular momentum recoupling coefficients [25].

Calculation of the two-body matrix elements for the interaction, however, is more involved if one moves to a general radial basis. The nucleon-nucleon interaction is defined

in relative coordinates. The oscillator basis is special, in that matrix elements in a relative oscillator basis, consisting of functions $\Psi_{nl}(\mathbf{r}_1 - \mathbf{r}_2)$, can readily be transformed to the two-body oscillator basis, consisting of functions $\Psi_{n_1 l_1}(\mathbf{r}_1)\Psi_{n_2 l_2}(\mathbf{r}_2)$, by the Talmi-Moshinsky transformation [29]. We therefore start from the two-body matrix elements $\langle cd; J|V|ab; J\rangle$ generated with respect to the oscillator basis, and only then carry out a change of basis in the two-body space [31].

Specifically, the change of basis for interaction two-body matrix elements is accomplished by the transformation

$$\langle \bar{c}\bar{d}; J|V|\bar{a}\bar{b}; J\rangle = \sum_{abcd}\langle a|\bar{a}\rangle\langle b|\bar{b}\rangle\langle c|\bar{c}\rangle\langle d|\bar{d}\rangle\,\langle cd; J|V|ab; J\rangle, \tag{4}$$

where we label single-particle orbitals for the oscillator basis by unbarred symbols $a = (n_a l_a j_a)$ and those for the Coulomb-Sturmian basis by barred symbols $\bar{a} = (\bar{n}_a \bar{l}_a \bar{j}_a)$. (See Ref. [25] for detailed definitions and normalization conventions.) The coefficients $\langle a|\bar{a}\rangle$ are obtained from the one-dimensional overlaps of the harmonic oscillator and Coulomb-Sturmian radial functions, $\langle R_{nl}|S_{\bar{n}l}\rangle = \int_0^\infty dr\, R_{nl}(b_{\mathrm{HO}}; r)S_{\bar{n}l}(b_{\mathrm{CS}}; r)$. It may be noted that the oscillator length b_{HO} — with respect to which the original oscillator two-body matrix elements of the interaction are represented — will in general be different from the length scale b_{CS} of the Coulomb-Sturmian functions — defining the basis for the many-body calculation.

The change-of-basis transformation in (4) is, in practice, limited to a finite sum, *e.g.*, with a shell cutoff $N_a, N_b, N_c, N_d \leq N_{\mathrm{cut}}$. The cutoff N_{cut} must be chosen high enough to ensure that the results of the subsequent many-body calculation are cutoff-independent, as verified by carrying out calculations with differing cutoffs. The accuracy obtained for a given cutoff may in general be expected to depend upon the oscillator and Coulomb-Sturmian length parameters defining the initial and final bases for the interaction, respectively, as well as upon the characteristics of the interaction (*e.g.*, softness), nuclear eigenstates, and observables under consideration.

The radius observables considered in the study of halo nuclei are the RMS radii of the point-nucleon distributions: the proton distribution radius r_p, the neutron distribution radius r_n, and the combined matter distribution radius r_m. The RMS radius of the proton, neutron, and matter distributions are related as $Ar_m^2 = Zr_p^2 + Nr_n^2$, and therefore only two out of three of these may be considered as independent observables. Although r_n is perhaps conceptually linked most naturally to neutron halo structure, r_p and r_m are most commonly

quoted, in recognition of experimental considerations (see Sec. III A).

The radii are all taken relative to the center of mass of the full set of nucleons, *i.e.*, protons and neutrons in aggregate, and are obtained from the expectation values of the relative square-radius operators defined in (A1). Much like the T_{rel} operator of (3), these are two-body operators which decompose into one-body and separable two body parts, involving $\sum_i \mathbf{r}_i^2$ and $\sum'_{ij} \mathbf{r}_i \cdot \mathbf{r}_j$, respectively, and evaluation of matrix elements proceeds similarly [25]. Specific relations needed for evaluating the two-body matrix elements of the proton and neutron relative square-radius operators with respect to an arbitrary basis may be found in the Appendix.

C. Basis length parameters and proton-neutron asymmetry

Any single-particle basis, including (1) or (2), has, as a free parameter, an overall length scale, which we may denote by b. For the oscillator basis, this is traditionally quoted as the oscillator energy $\hbar\Omega$, where

$$b(\hbar\Omega) = \frac{(\hbar c)}{[(m_N c^2)(\hbar\Omega)]^{1/2}}. \tag{5}$$

In deference to the convention of presenting NCCI results as a function of $\hbar\Omega$ as the basis parameter, we nominally carry over this relation to define an $\hbar\Omega$ parameter for general radial bases. This $\hbar\Omega$ has no direct physical meaning as an energy scale for the Coulomb-Sturmian basis. However, the inverse square-root dependence remains, so that a factor of two change in $\hbar\Omega$ still describes a factor of $\sqrt{2}$ change in length scale (illustrated for both harmonic oscillator and Coulomb-Sturmian bases by the dotted curves in Fig. 2).

Beyond an overall length scale, there is additional freedom in length scales which may be exploited in constructing the basis. The many-body basis states (antisymmetrized product states) constructed from a single-particle basis are orthonormal so long as the single-particle states are orthonormal. Orthogonality for single-particle states of different l or j follows entirely from the angular and spin parts of the wave function. Only orthogonality *within* the space of a given l and j follows from the radial functions, *e.g.*, for the Coulomb-Sturmian functions, $\langle n'l'j'|nlj\rangle = \left[\int dr\, S_{n'l}(b;r)\, S_{nl}(b;r)\right]\delta_{l'l}\delta_{j'j}$. We are therefore free to choose b independently, firstly, for each l space (or j space), as b_l (or b_{lj}), and, secondly, for protons and neutrons, as b_p and b_n.

The first observation raises the possibility, still to be explored, of obtaining significant

improvements in the efficacy of the basis by optimizing the l-dependence of the length parameter. For now, we follow the choice of Ref. [25] for the Coulomb-Sturmian functions, which is motivated by more closely matching the Coulomb-Sturmian functions to the oscillator functions in the small-r region. Specifically, b_l is chosen so that the first node of the $n = 1$ Coulomb-Sturmian function for each l aligns with the first node of the $n = 1$ oscillator function for that l, which, from the zeros of the Laguerre polynomials, yields the prescription

$$b_l = \sqrt{\frac{2}{2l + 3}} b(\hbar\Omega). \tag{6}$$

It is this prescription for b_l which is shown in Fig. 2(b).

The second observation raises the possibility of proton-neutron asymmetric length scales, which might be advantageous for nuclei with significant disparities between the proton and neutron distributions, in particular, halo nuclei. Therefore, in the present work, we adopt

$$b_{l,p} = \sqrt{\frac{2}{2l + 3}} b(\hbar\Omega) \qquad b_{l,n} = \beta \sqrt{\frac{2}{2l + 3}} b(\hbar\Omega), \tag{7}$$

where β sets an overall relative scale b_n/b_p. For example, if the solid and dotted curves in Fig. 2(b) are taken to represent the proton and neutron radial functions, respectively, then the figure illustrates the case in which $\beta \equiv b_n/b_p = \sqrt{2} \approx 1.414$.

III. CALCULATIONS FOR He ISOTOPES

A. Experimental background

The isotopes [6]He and [8]He are interpreted as halo nuclei, consisting of a neutron halo surrounding an α core, as reviewed in, *e.g.*, Refs. [11, 12]. The last neutrons in these isotopes are only weakly bound, with two-neutron separation energies of $0.97\,\text{MeV}$ and $2.14\,\text{MeV}$, respectively. The halo structure is most notably evident in a sudden increase in the RMS radii of both the proton and matter distributions along the isotopic chain, summarized in Table I (see also Fig. 8 below). Moving from [4]He to [6]He, the measured r_p increases by $\sim 32\%$. This may be understood as resulting from the recoil of the α core against the halo neutrons — *i.e.*, the presence of the halo neutrons on average displaces the center of mass of the nucleus away from the center of mass of the α particle — as well as possibly receiving a contribution from core polarization or "swelling" [32]. An even greater, though less precisely

known, increase in r_m reflects the extended halo neutron distribution. The measured proton and matter radii for ^{8}He are comparable to those for ^{6}He. It is worth briefly summarizing the experimental situation — the origins of the reported radii and their differences — before using them as a baseline for comparison with the present *ab initio* predictions.

The proton radii r_p are obtained experimentally with comparatively high precision (better than 0.02 fm). The charge radius of the stable isotope ^{4}He can be measured directly from electron scattering [33]. The charge radii of the unstable isotopes ^{6,8}He are determined indirectly from isotope shift data [34, 35] in combination with precise mass measurements [36]. The RMS radius of the point-proton distribution is then deduced, after hadronic physics corrections [37], from the nuclear charge radius. The experimental values for r_p from the evaluation by Lu *et al.* [32] are 1.462(6) fm for ^{4}He, 1.934(9) fm for ^{6}He, and 1.881(17) fm for ^{8}He.

The matter radii r_m are obtained with considerably greater uncertainties, from either nuclear interaction cross sections [38] or proton-nucleus elastic scattering data [39]. These methods yield model-dependent and often contradictory results along the He isotopic chain.

Analyses of the interaction cross section data for ^{4}He via the Glauber model yield either $r_m = 1.57(4)$ fm [40] or 1.63(3) fm [41], depending on assumptions regarding the parameters for the orbitals defining the matter distribution. For ^{4}He, r_p and r_m should be essentially identical by isospin symmetry. However, these reported r_m values are substantially larger than and inconsistent, at the stated uncertainties, with the measured $r_p = 1.462(6)$ fm. On the other hand, elastic scattering yields $r_m = 1.49(3)$ fm [39], consistent with r_p.

For ^{6}He, the same Glauber analyses of the interaction cross section data yield $r_m = 2.48(4)$ fm [40] or 2.33(4) fm [41]. However, a few-body analysis, explicitly considering ^{6}He as a correlated system consisting of a core plus two valence neutrons, suggests a significantly larger value $r_m = 2.71(4)$ fm [42]. The elastic scattering data yield either $r_m = 2.30(7)$ fm in an analysis assuming Gaussian asymptotics, or 2.45(10) fm in an alternative analysis with extended (Hankel function) tails [39].

Finally, for ^{8}He, the Glauber analyses of interaction cross section data yield $r_m = 2.52(3)$ fm [40] or 2.49(4) fm [41]. The analyses of elastic scattering data assuming different asymptotics yield $r_m = 2.45(7)$ fm or 2.53(8) fm [39], respectively.

Experimental ranges for r_m encompassing the extreme values (including uncertainties) of the reported analyses, and identical to those adopted by Lu *et al.* [32], are 1.46–1.66 fm

for ^{4}He, 2.23–2.75 fm for ^{6}He, and 2.38–2.61 fm for ^{8}He. When we compare with theory, it is worth bearing in mind that the narrower range of experimental r_m values indicated for ^{8}He, relative to ^{6}He, does not represent fundamentally smaller experimental or model uncertainties, but rather simply a narrower range of attempted model analyses. The few-body analysis reported for ^{6}He [42] is responsible for raising the upper bound of the experimental range for this nucleus by 0.2 fm, while no corresponding analysis is available for ^{8}He.

B. NCCI calculations

We carry out calculations for the isotopes ^{4,6,8}He using both the harmonic oscillator and Coulomb-Sturmian bases. These calculations are based on the JISP16 nucleon-nucleon interaction [43], plus Coulomb interaction. The bare interaction is used, *i.e.*, without renormalization. The proton-neutron M-scheme code MFDn [44–46] is employed for the many-body calculations.

The harmonic oscillator many-body basis is normally truncated according to the $N_{\max}$ scheme, which limits the total number of oscillator quanta as $N_{\mathrm{tot}} \equiv \sum_i N_i = \sum_i (2n_i + l_i) \leq N_0 + N_{\max}$, where N_0 is the minimal number of oscillator quanta for the given number of protons and neutrons. We formally carry this truncation over to the Coulomb-Sturmian basis for the calculations in the present work, although, as noted in Sec. II A, $N \equiv 2n + l$ no longer has significance as an energy with respect to a mean field, nor does it lead to the exact factorization of center-of-mass motion which is obtained with an oscillator basis in $N_{\max}$ truncation (*e.g.*, Ref. [3]). Results are calculated with truncations up to $N_{\max} = 16$ for ^{4,6}He and $N_{\max} = 14$ for ^{8}He, for both the harmonic oscillator and Coulomb-Sturmian bases.

C. Results for ^{4}He

Let us first consider the calculations for ^{4}He, as the baseline case. The computed ground state energies and proton radii are summarized in Fig. 3. Recall that there is no physical meaning in comparing $\hbar\Omega$ values directly between oscillator and Coulomb-Sturmian bases, but that ratios of $\hbar\Omega$ values within a basis are meaningful, serving to indicate the ratio of length scales (Sec. II C). Results are therefore shown consistently over a factor of four range
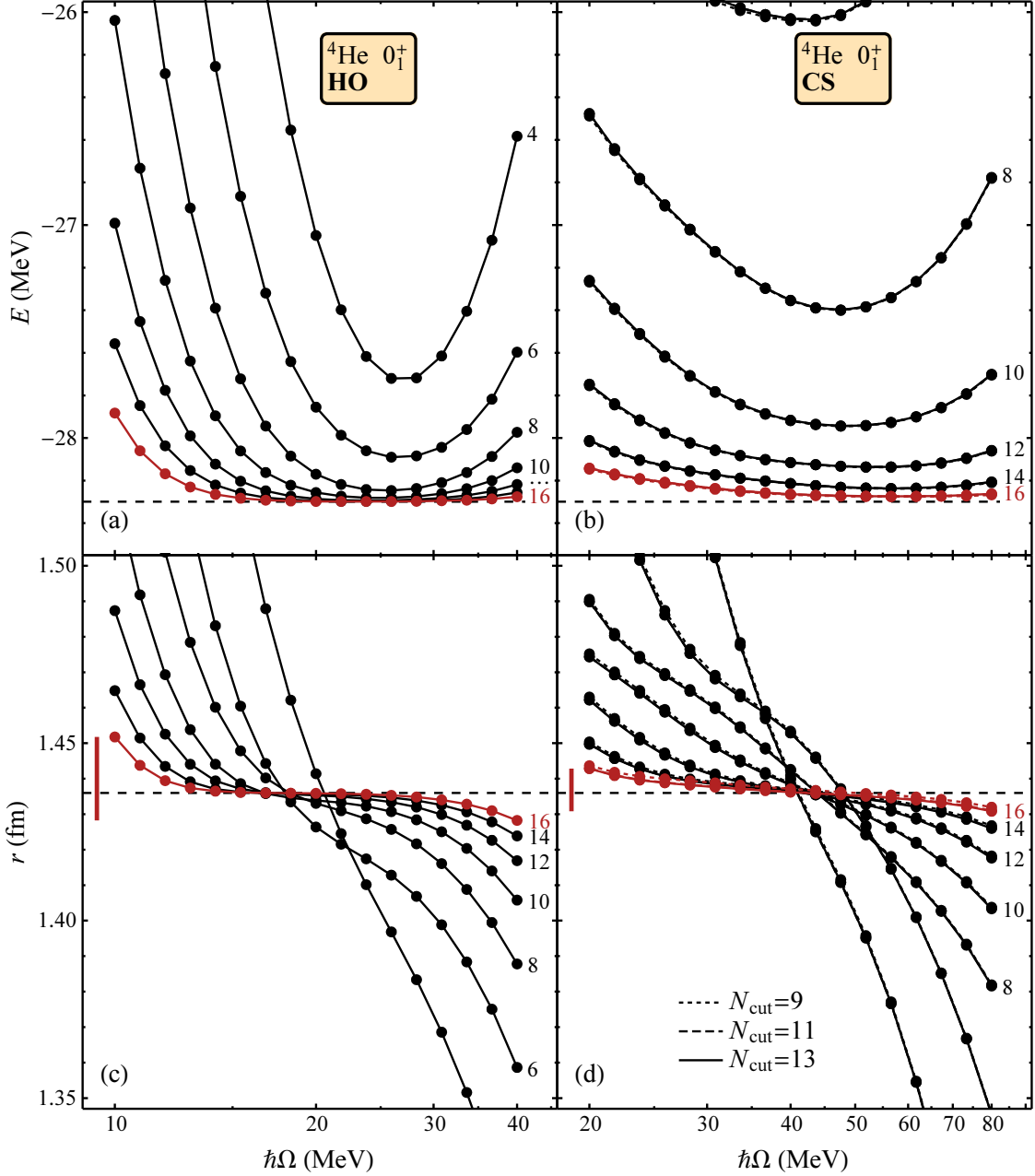
FIG. 3: The calculated ^{4}He ground state energy (top) and RMS proton radius r_p (bottom), using the conventional oscillator (left) and Coulomb-Sturmian (right) bases. These are shown as functions of the basis $\hbar\Omega$ parameter, for $N_{\max} = 4$ to 16 (as labeled), and for transformation cutoffs $N_{\mathrm{cut}} = 9$, 11, and 13 (Coulomb-Sturmian basis only, indicated by dashing, curves nearly indistinguishable). The converged values obtained with the JISP16 interaction are indicated by dashed horizontal lines. The spreads in radius values over this $\hbar\Omega$ range, at the highest $N_{\max}$, are indicated by vertical bars (at bottom).

in $\hbar\Omega$, *i.e.*, representing a doubling in basis length scale, for all bases in the present work, to facilitate comparison across different bases, and a logarithmic scale is used for $\hbar\Omega$.

Energy convergence is reached for the harmonic oscillator basis, as evidenced by approximate N_{max} and $\hbar\Omega$ independence of the higher N_{max} results over a range of $\hbar\Omega$ values, in Fig. 3(a,b). Convergence is obtained at the $\sim 10\,\text{keV}$ level by $N_{max} = 14$. The binding energies for ^{4}He computed with the Coulomb-Sturmian basis lag significantly behind those obtained with the oscillator basis, by about two steps in N_{max}. This should perhaps not be surprising, given that ^{4}He is tightly bound, and the structure can thus be expected to be driven by short-range correlations rather than asymptotic properties.

It is important to note that stability with respect to the cutoff in the change-of-basis transformation (4) has been obtained — calculations with $N_{cut} = 9$, 11, and 13 are virtually indistinguishable in Fig. 3(b,d). The transformation has been carried out from oscillator basis interaction matrix elements at $\hbar\Omega_{int} = 40\,\text{MeV}$.

Convergence of the computed RMS radii, for both the oscillator and Coulomb-Sturmian bases, is again indicated by approximate N_{max} and $\hbar\Omega$ independence over a range of $\hbar\Omega$ values, which appears as a shoulder in the curves of Fig. 3(c,d). The vertical bars in Fig. 3(c,d) indicate the spread in radii obtained (at the highest N_{max}) over the range of $\hbar\Omega$ plotted, to aid comparison. The $\hbar\Omega$ dependence for the Coulomb-Sturmian calculations appears to be moderately shallower over the range shown, which spans a factor of four in $\hbar\Omega$ for each basis. However, it should be borne in mind that, since the slopes of the curves in Fig. 3(c,d) vary significantly with $\hbar\Omega$, the spread in radii is sensitive to the particular range of $\hbar\Omega$ values chosen, *e.g.*, whether this range is centered on the variational minimum of the energy calculations or on the crossover point (it is more simply chosen for purposes of presentation in this and subsequent figures) and how wide a range is considered.

D. Results for ^{6,8}He

Let us now consider the calculations for the halo nuclei ^{6,8}He. The computed ground state energies, proton radii, and matter radii are shown in Figs. 4 and 5. Results are included (at right in each figure) for a Coulomb-Sturmian basis with proton-neutron asymmetric length scales (Sec. II C) in the ratio $\beta \equiv b_n/b_p = 1.414$, which is comparable to the ratio r_n/r_p of neutron and proton distribution radii for these nuclei.
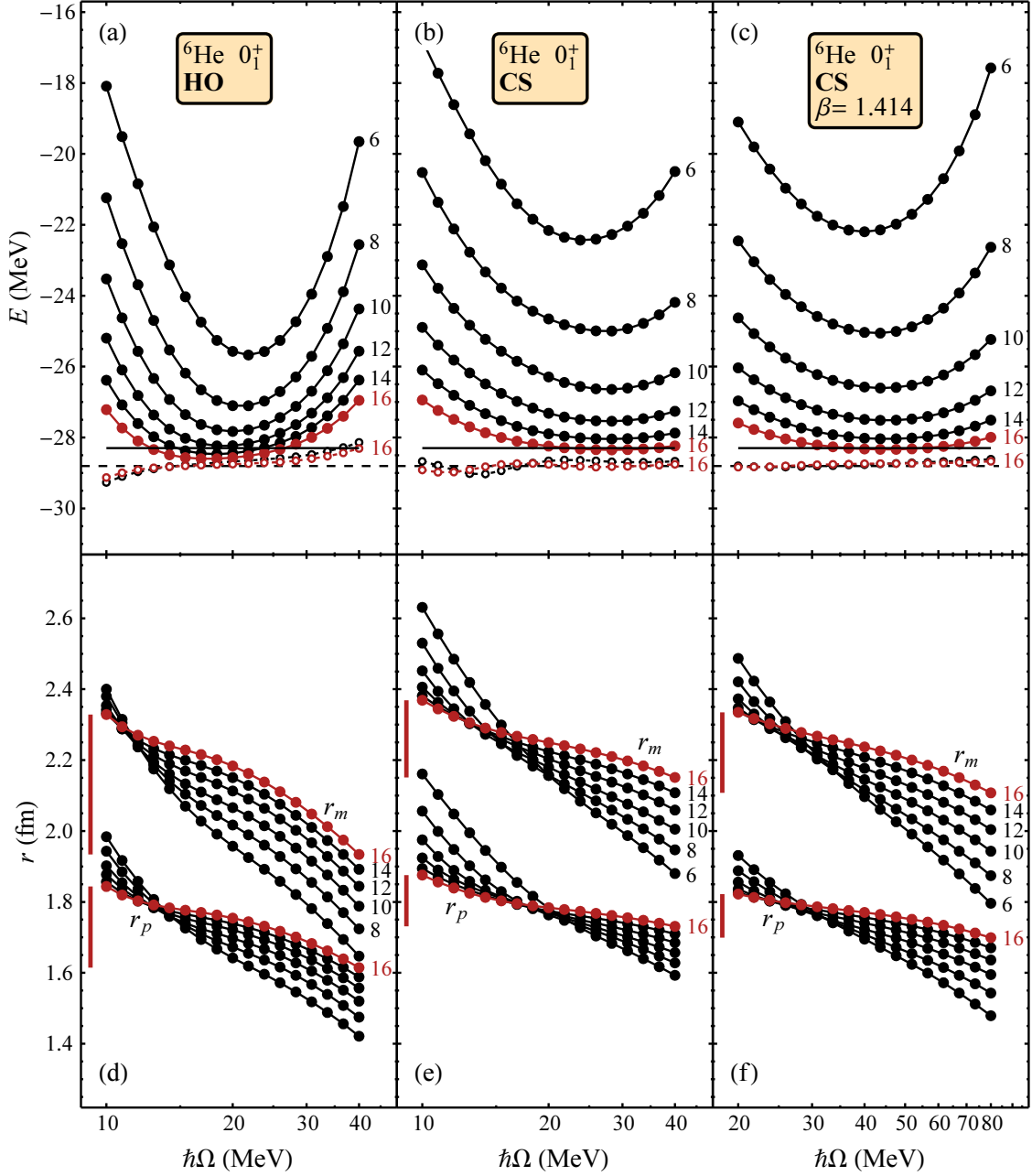
FIG. 4: The calculated ^{6}He ground state energy (top) and RMS proton radius r_p and matter radius r_m (bottom), using the conventional oscillator basis (left), Coulomb-Sturmian basis (center), and proton-neutron asymmetric Coulomb-Sturmian basis with $\beta = 1.414$ (right). These are shown as functions of the basis $\hbar\Omega$ parameter, for $N_{\max} = 6$ to 16 (as labeled). Exponentially extrapolated energies from the present calculations are indicated by open symbols, the best extrapolated energy from Ref. [47] is indicated by the dashed horizontal line, and the ^{4}He + $2n$ breakup threshold obtained with JISP16 [47] is marked by the solid horizontal line (at top). The spreads in radii over this $\hbar\Omega$ range, at the highest $N_{\max}$, are indicated by vertical bars (at bottom).
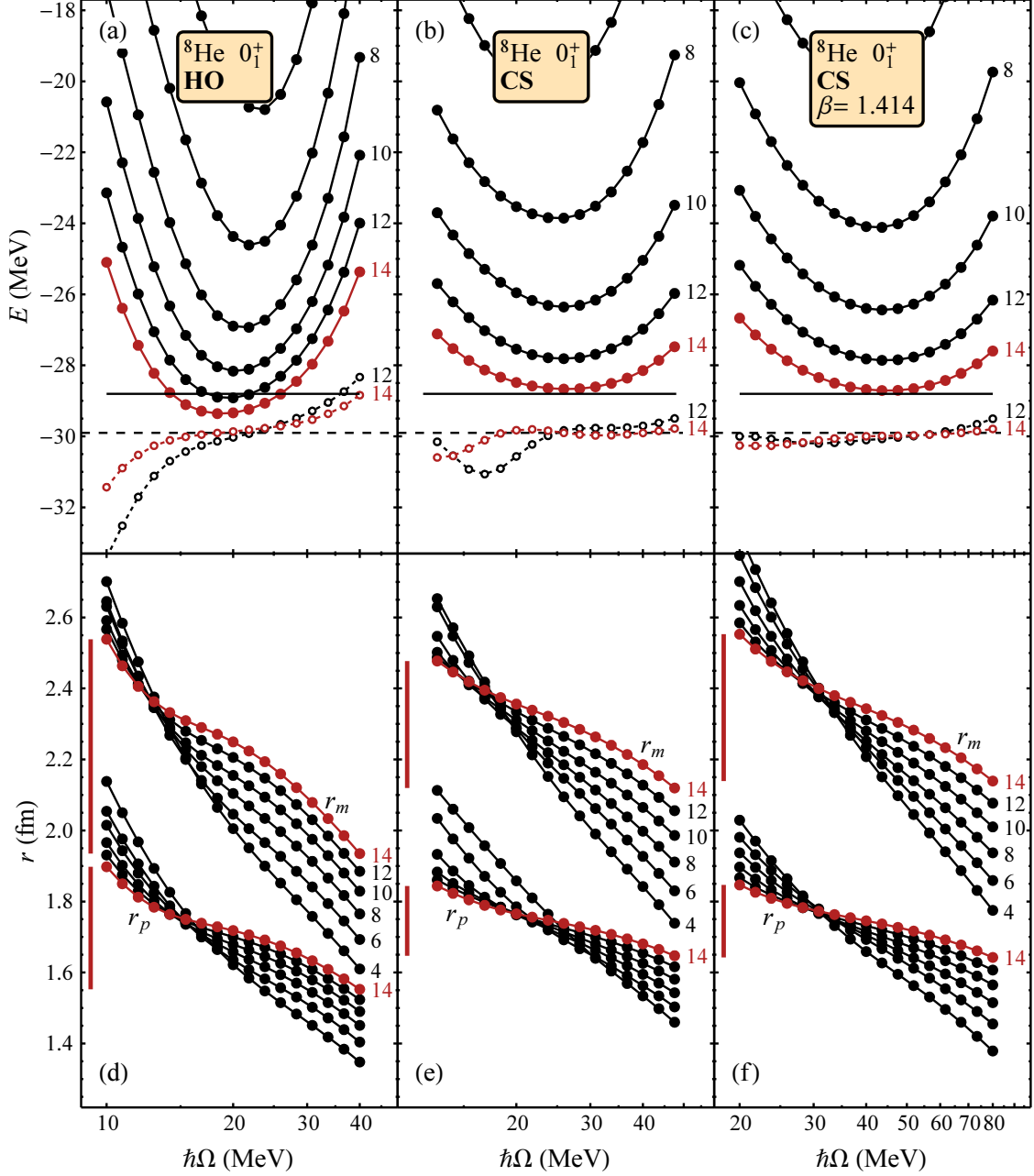
FIG. 5: The calculated ^{8}He ground state energy (top) and RMS proton radius r_p and matter radius r_m (bottom), using the conventional oscillator basis (left), Coulomb-Sturmian basis (center), and proton-neutron asymmetric Coulomb-Sturmian basis with $\beta = 1.414$ (right). These are shown as functions of the basis $\hbar\Omega$ parameter, for $N_{\max} = 4$ to 14 (as labeled). Exponentially extrapolated energies from the present calculations are indicated by open symbols, the best extrapolated energy from Ref. [47] is indicated by the dashed horizontal line, and the ^{6}He $+ 2n$ breakup threshold obtained with JISP16 [47] is marked by the solid horizontal line (at top). The spreads in radii over this $\hbar\Omega$ range, at the highest $N_{\max}$, are indicated by vertical bars (at bottom).

Energy convergence in the Coulomb-Sturmian basis lags that of the harmonic oscillator basis, but less dramatically than seen above for ^{4}He. A basic three-point exponential extrapolation [6] of the energy with respect to N_{max}, at each $\hbar\Omega$ value, is indicated by the open symbols in Figs. 4 (top) and 5 (top). The extrapolated energy is remarkably $\hbar\Omega$-independent in the $\beta = 1.414$ calculations, although it should be noted that there is still some N_{max} dependence as well. The extrapolated energy appears to be approximately consistent with the harmonic oscillator extrapolations. (The dashed line indicates the best extrapolated value from harmonic oscillator basis calculations from Ref. [47], up to $N_{max} = 18$ for ^{6}He or $N_{max} = 14$ for ^{8}He, using a three-point extrapolation at the $\hbar\Omega$ determined by the variational energy minimum, yielding binding energies of $28.803(6)$ MeV and $29.9(2)$ MeV for these isotopes, respectively.) However, such extrapolations must be viewed with caution, as both theoretical arguments and empirical studies suggest that functional forms other than an exponential in N_{max} may be more appropriate, over at least portions of the $\hbar\Omega$ range [7–9].

Since ^{6}He and ^{8}He are weakly bound neutron halo nuclei, small differences in the calculated binding energy may be expected to have large effects on the calculated structure, in particular, whether or not a bound state is even obtained. While the JISP16 interaction does bind both ^{6}He and ^{8}He against two-neutron decay, it does so with two-neutron separation energies of only $0.504(6)$ MeV and $1.1(2)$ MeV, respectively, based on the best extrapolations of Ref. [47], thus underbinding both nuclei relative to the experimental values (see Sec. III A). The $2n$ thresholds based on the binding energies obtained with the JISP16 interaction are indicated in Figs. 4 (top) and 5 (top) by the solid horizontal line. For ^{6}He, convergence of the energies to the point that the variational minimum (with respect to $\hbar\Omega$) lies below this threshold is obtained between $N_{max} = 12$ and 14 for the oscillator basis calculations [Fig. 4(a)], or between $N_{max} = 14$ and 16 for the Coulomb-Sturmian basis calculations [Fig. 4(b,c)]. For ^{8}He, the variational minimum falls below the $2n$ threshold between $N_{max} = 10$ and 12 for the calculations with the oscillator basis [Fig. 5(a)], while the variational minimum energies obtained with the Coulomb-Sturmian basis are still just shy of the threshold for the largest space considered ($N_{max} = 14$). In making these comparisons, it should be noted that there is little difference in the variational mimimum energies obtained with the $\beta = 1$ or $\beta = 1.414$ calculations, which, e.g., differ by only ~ 0.01 MeV for ^{6}He at $N_{max} = 16$ [Fig. 4(b,c)] or ~ 0.04 MeV for ^{8}He at $N_{max} = 14$ [Fig. 5(b,c)]. For both isotopes, the greatest variational gain in binding energy is actually obtained for an intermediate value

for the ratio of proton and neutron basis length scales, $\beta \approx 1.1$–1.2 (not shown).

Comparing the results for radii obtained with the different bases, for ^{6}He [Fig. 4 (bottom)] and ^{8}He [Fig. 5 (bottom)], we see that Coulomb-Sturmian calculations (for either $\beta = 1$ or $\beta = 1.414$) again yield a moderately shallower $\hbar\Omega$ dependence than obtained with the harmonic oscillator basis over a wider interval in $\hbar\Omega$. On the other hand, the harmonic oscillator basis results give more of an appearance of localized shouldering.

IV. RADIUS ANALYSIS

In examining the dependence of the calculated radii for the He isotopes (Figs. 3–5) on $N_{\max}$ and $\hbar\Omega$, there is qualitatively similar behavior, across the bases. The curves for the radii as functions of $\hbar\Omega$, at different $N_{\max}$, give the appearance of approximately "converging" to a common intersection point, at an $\hbar\Omega$ value somewhat below that of the variational minimum in the energy. The observation that, at lower $\hbar\Omega$, the calculated radii decrease with $N_{\max}$, while, at higher $\hbar\Omega$, the calculated radii increase with $N_{\max}$, leaving the calculated radius essentially independent of $N_{\max}$ at the crossover $\hbar\Omega$, might be taken to suggest that the crossover provides a reasonable estimate of the true converged radius.

It was therefore proposed in Refs. [5, 14] that the radius can be estimated — even before convergence is well-developed — by the crossover point. (Closer inspection reveals that there is no common intersection point in any strict sense: if we consider the curves obtained for successive values of $N_{\max}$, the $\hbar\Omega$ value at which these curves cross drifts by several MeV as $N_{\max}$ increases, generally towards lower $\hbar\Omega$. Nonetheless, we may consider crossovers between the curves at successive values of $N_{\max}$.) This is an admittedly *ad hoc* prescription, rather than a theoretically motivated extrapolation. However, while the approach was originally presented simply in the context of NCCI calculations with the harmonic oscillator basis, we can now test this approach further and verify consistency by comparing results obtained from bases with substantially different underlying single-particle radial functions.

We can most directly test the crossover prescription — for both oscillator and Coulomb-Sturmian bases — in the case of ^{4}He, where the final converged value is known. The crossover radii are shown as a function of $N_{\max}$, for both bases, in Fig. 6. The curves (of radius as a function of $\hbar\Omega$ at fixed $N_{\max}$) used in deducing these crossovers are computed by cubic interpolation of the calculated data points at different $\hbar\Omega$. The crossovers already serve to
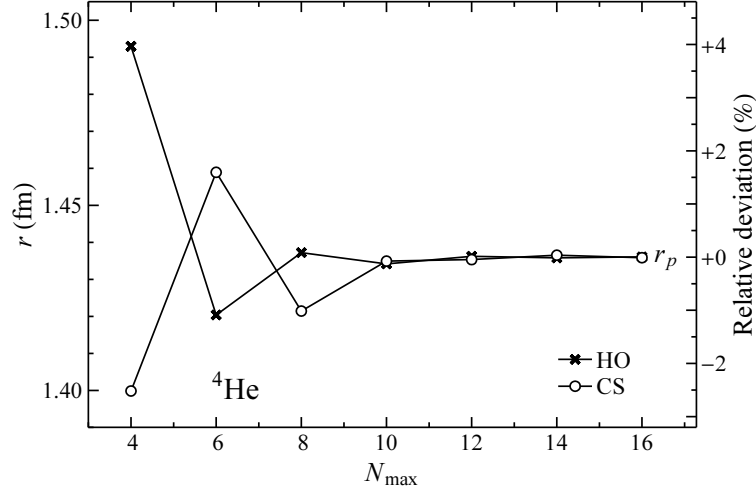
FIG. 6: The ^{4}He ground state RMS proton radius r_p, as estimated from the crossover point (see text), calculated for the harmonic oscillator and Coulomb-Sturmian bases (as indicated in the legend). The relative deviations from the converged value may be read from the right-hand axis.

estimate the final converged value to within ~ 0.05 fm at $N_{\mathrm{max}} = 6$.[1] The main merit of the approach appears to be that, in the face of calculated values for the radius which depend smoothly and strongly on the basis parameter $\hbar\Omega$, it appears to select out the converged value more rapidly than, *e.g.*, simply choosing to evaluate the radius at the $\hbar\Omega$ value which yields the variational minimum in the energy.

The extracted crossover radii for ^{6,8}He are shown, as functions of N_{max}, in Fig. 7. The radii obtained for the Coulomb-Sturmian calculations with different ratios of neutron and proton length scales ($\beta = 1$ and 1.414) track each other closely from $N_{\mathrm{max}} \approx 8$ onward, agreeing with each other to within ~ 0.1 fm. For r_p, the values are stable with respect to N_{max} and agree with the values obtained from the harmonic oscillator basis crossover as well. For r_m, it appears that the values might be drifting systematically upward with N_{max}, although they do remain within an ~ 0.2 fm range from $N_{\mathrm{max}} = 8$ to the highest N_{max} calculated. Therefore, although we can extract a result based on this highest N_{max} (as discussed below), it is not possible to give a definitive value for r_m.

An overview of the predicted evolution of the radius observables along the He isotopic chain, and a comparison with experimental values, is provided in Fig. 8. (Although the

---

[1] A similar crossover analysis, not shown in Fig. 6, may be carried out for the matter radius of ^{4}He, yielding marginally smaller values (by ~ 0.003 fm), since the neutrons are not subject to Coulomb repulsion.
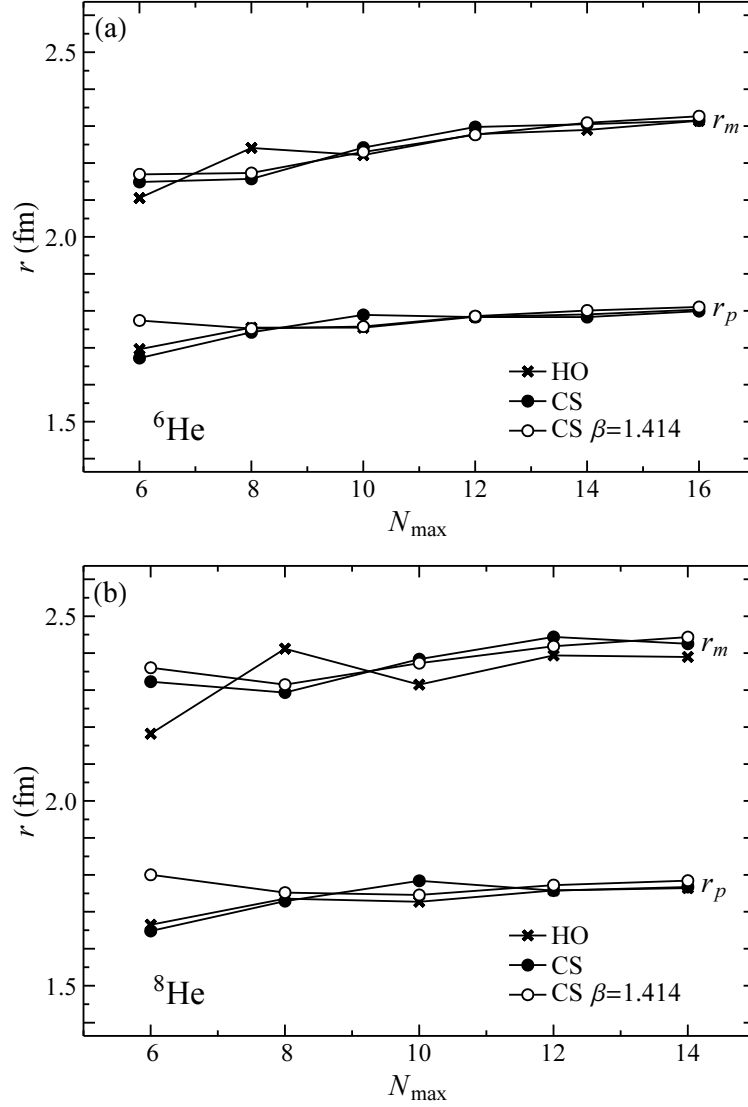
FIG. 7: The (a) ^{6}He and (b) ^{8}He ground state RMS proton radius r_p (lower curves) and matter radius r_m (upper curves), as estimated from the crossover point (see text), calculated for the harmonic oscillator basis, Coulomb-Sturmian basis, and proton-neutron asymmetric Coulomb-Sturmian basis with $\beta = 1.414$ (as indicated in the legend).

dependence of the extracted crossover radius on $N_{\max}$ was shown in Figs. 6 and 7, here it is helpful to directly see the stability of each radius with respect to $N_{\max}$, by overlaying the results obtained for the three highest successive $N_{\max}$ values, with the largest symbol indicating the result for the highest $N_{\max}$ value.) The radii obtained at the highest $N_{\max}$, for each basis, are summarized in Table I. For each radius considered, the values obtained from the calculations with different bases are consistent to within ~ 0.02 fm, or ~ 0.05 fm

TABLE I: The ^{4,6,8}He proton and matter radii, as estimated from the crossover point at the highest $N_{\max}$ calculated ($N_{\max} = 16$ for ^{4,6}He and $N_{\max} = 14$ for ^{8}He), for the harmonic oscillator basis (HO), Coulomb-Sturmian basis (CS), and proton-neutron asymmetric Coulomb-Sturmian basis with $\beta = 1.414$ (CS β). Experimental values or ranges (see Sec. III A) are also given. All radii are in fm.

		^{4}He	^{6}He	^{8}He
r_p	HO	1.4361	1.803	1.764
	CS	1.4358	1.799	1.767
	CS β	—	1.810	1.784
	Expt.	1.462(6)	1.934(9)	1.881(17)
r_m	HO	1.4335	2.314	2.390
	CS	1.4332	2.315	2.425
	CS β	—	2.327	2.443
	Expt.	1.46–1.66	2.23–2.75	2.38–2.61

in the case of the ^{6}He matter radius.[2] The radii for these light nuclei are also accessible to other *ab initio* methods — results have recently been reported based on the effective interaction hyperspherical harmonic (EIHH) method [52] and Green's function Monte Carlo (GFMC) method [32] and could be extracted from calculations based upon the no-core shell model/resonating group method (NCSM/RGM) [53] — suggesting the possibility of benchmarking calculations carried out for the same interaction under different calculational approaches and extrapolation schemes [26, 27].

The proton radius calculated for ^{4}He matches the experimental result to within ~ 0.02 fm. Indeed, this is perhaps an unreasonably good level of agreement to expect from imperfectly

---

[2] The present values for the ^{6,8}He radii are consistent with estimates [48] obtained, from the same NCCI calculations, by infrared oscillator basis extrapolation methods of the type proposed in Refs. [8, 9, 27]. (The detailed results are sensitive to the range of $N_{\max}$ and $\hbar\Omega$ values included in the extrapolation procedure, as well as to the prescription used for the infrared cutoff parameter [49].) The present values are also consistent with estimates $r_p = 1.84(8)$ fm and $r_m = 2.43(19)$ fm obtained from calculations for ^{6}He using Woods-Saxon bases, under the JISP16 interaction, in Refs. [50, 51].
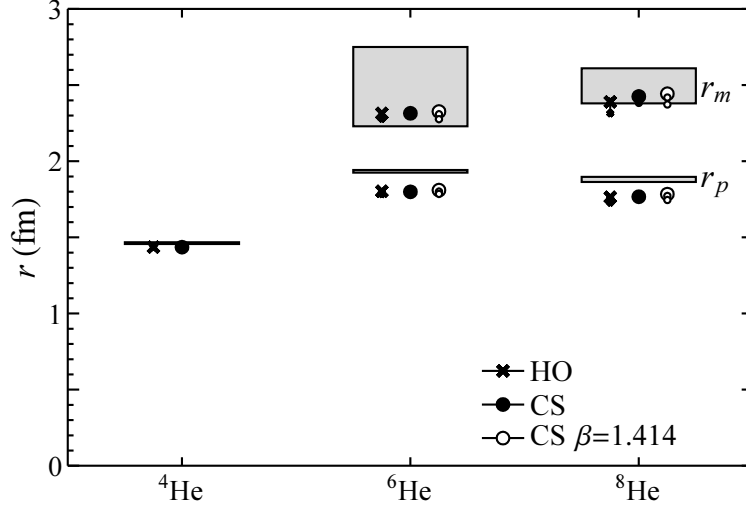
FIG. 8: The ^{4}He proton radius and ^{6,8}He proton and matter radii, as estimated from the crossover point, for the harmonic oscillator basis, Coulomb-Sturmian basis, and proton-neutron asymmetric Coulomb-Sturmian basis with $\beta = 1.414$. For each of these bases, the extracted radii are shown for the highest three successive $N_{\max}$ values ($12 \leq N_{\max} \leq 16$ for ^{4,6}He or $10 \leq N_{\max} \leq 14$ for ^{8}He), in some cases visually indistinguishable, with the largest symbol indicating the highest $N_{\max}$ value. Experimental values or ranges are shown as horizontal bands.

known internucleon interactions. In any case, it is at the same scale as systematic uncertainties in the experimental corrections for the proton size from hadronic physics [32].

The present calculations with the JISP16 interaction qualitatively reproduce the observed jump in radii. From ^{4}He to ^{6}He, the calculated r_p increases by 25% — quantitatively somewhat short of the measured 32% increase — then remains essentially unchanged for ^{8}He. The calculated r_m increases by 62% from ^{4}He to ^{6}He, again remaining essentially unchanged for ^{8}He. These matter radii are in good agreement with the elastic scattering measurements (Sec. III A), $i.e.$, with the lower end of the experimental range.

V. CONCLUSION

The present work is, in various respects, an investigation of computational methods (alternative radial bases for the NCCI approach), an investigation of analysis methods (for extracting an estimator of the converged radius from still-unconverged calculations), and an investigation of a physical problem (*ab initio* prediction of halo structure in the He isotopes).

From the computational viewpoint, the NCCI approach has been applied with bases incorporating realistic exponential asymptotics (the Coulomb-Sturmian functions) and proton-neutron asymmetry (in recognition of the physical asymmetry of the system). Calculations with the Coulomb-Sturmian basis are found to be valuable in predicting RMS radius observables for the He isotopes subject to the JISP16 interaction. Convergence of the binding energy is moderately slower than with the harmonic oscillator basis. This appears to be at least partially offset by more stable extrapolation properties when the basic exponential extrapolation scheme is used. Calculations of the RMS radii of ^{6,8}He appear to show improved $\hbar\Omega$ independence with the Coulomb-Sturmian basis. However, for both observables, more complete, theoretically motivated extrapolation studies are needed.

It would seem that a principal underlying challenge to devising an appropriate expansion basis is the compromise involved in addressing both the core nucleons and the halo nucleons with basis functions sharing the same length parameter, and thus the same rate of exponential fall-off in the asymptotic region. A single-particle basis encompassing functions with differing length scales (as encountered in atomic electron-structure calculations [54]) might be expected to provide greater efficiency in describing halo structure. Further optimization of the Coulomb-Sturmian basis is also likely possible through variation of the l dependence of the length parameters, potentially yielding improved convergence (analogous optimizations are again important for rapid convergence in electron-structure calculations).

In the present work, perhaps the most direct benefit of going beyond the oscillator basis lies simply in being able to compare calculations obtained with qualitatively different basis sets, and thereby to verify the robustness of the estimated observable values extracted from still-unconverged calculations. The crossover prescription for radius observables, although *ad hoc*, is found to yield consistent results, to within ~ 0.02–0.05 fm, between bases with substantially different underlying single-particle radial functions.

These results give estimates for the proton and matter radii of the He halo nuclei, based on *ab initio* calculations, with the JISP16 interaction. The distinctive trend in radii along the He isotopic chain, indicative of the onset of halo structure, is qualitatively reproduced. More quantitatively, the proton radii of the halo isotopes are underestimated, relative to experiment, while the calculated matter radii favor the lower end of the experimental range.

Appendix A: Proton and neutron squared-radius operators

The RMS radii of the point-nucleon proton, neutron, or matter distributions, relative to the center of mass (Sec. II), are calculated as $r_p \equiv \langle r_p^2 \rangle^{1/2}$, $r_n \equiv \langle r_n^2 \rangle^{1/2}$, or $r_m \equiv \langle r_{\mathrm{rel}}^2 \rangle^{1/2}$, in terms of relative mean squared radius operators, which are defined by [52]

$$
\begin{aligned}
r_p^2 &= \frac{1}{N_p} \sum_i \delta_{p,i} (\mathbf{r}_i - \mathbf{R})^2 \\
r_n^2 &= \frac{1}{N_n} \sum_i \delta_{n,i} (\mathbf{r}_i - \mathbf{R})^2 \\
r_{\mathrm{rel}}^2 &= \frac{1}{A} \sum_i (\mathbf{r}_i - \mathbf{R})^2,
\end{aligned}
\tag{A1}
$$

in terms of the center-of-mass position operator

$$
\mathbf{R} = \frac{1}{A} \sum_i \mathbf{r}_i,
\tag{A2}
$$

where we define the shorthands $\delta_{p,i} = \frac{1}{2}(1 + \tau_{z,i})$ and $\delta_{n,i} = \frac{1}{2}(1 - \tau_{z,i})$ (with $\tau_z = +1$ for protons and -1 for neutrons) to select proton and neutron indices, respectively, and we denote the proton and neutron numbers by $N_p (\equiv Z)$ and $N_n (\equiv N)$ to provide greater uniformity between the expressions for the proton and neutron radii below. The operators in (A1) are two-body operators, due to the subtraction of the center-of-mass coordinate. Thus, in order to calculate their expectation values within a many-body wave function, the two-body matrix elements of these operators are required, with respect to the basis for the

calculation. In this appendix, we summarize certain operator relations needed for evaluating the two-body matrix elements of these operators.

The r_{rel}^2 operator, as defined in (A1), can be reexpressed in forms more suitable for evaluation of two-body matrix elements, as outlined in Appendix A of Ref. [25]. On the one hand, r_{rel}^2 can be expressed in the standard form for a two-body operator, $i.e.$, as a double sum over distinct particle indices, as

$$r_{\mathrm{rel}}^2 = \frac{1}{2A^2} \sideset{}{'}\sum_{ij} (\mathbf{r}_i - \mathbf{r}_j)^2, \tag{A3}$$

which we will use below. On the other hand, expanding the square in (A1) or (A3) gives an alternate expression for r_{rel}^2 in terms of one-body and separable two-body parts

$$r_{\mathrm{rel}}^2 = \frac{(A-1)}{A^2} \sum_i r_i^2 - \frac{1}{A^2} \sideset{}{'}\sum_{ij} \mathbf{r}_i \cdot \mathbf{r}_j. \tag{A4}$$

This latter expression may be used to evaluate the two-body matrix elements $\langle cd; J | r_{\mathrm{rel}}^2 | ab; J \rangle$ in a straightforward fashion, from the radial integrals of the r and r^2 operators with respect to the given single-particle basis, as elaborated in Sec. III D of Ref. [25].

The two-body matrix elements of the operators r_p^2 and r_n^2 may, conveniently, be deduced from those already obtained for the operator r_{rel}^2. To establish the relationship, it is helpful to first define the restrictions of r_{rel}^2 to the proton-proton, proton-neutron, and neutron-neutron sectors

$$r_{\mathrm{rel},pp}^2 = \frac{1}{2A^2} \sideset{}{'}\sum_{ij} \delta_{p,i} \delta_{p,j} (\mathbf{r}_i - \mathbf{r}_j)^2.$$

$$r_{\mathrm{rel},pn}^2 = \frac{1}{2A^2} \sideset{}{'}\sum_{ij} (\delta_{p,i} \delta_{n,j} + \delta_{n,i} \delta_{p,j})(\mathbf{r}_i - \mathbf{r}_j)^2. \tag{A5}$$

$$r_{\mathrm{rel},nn}^2 = \frac{1}{2A^2} \sideset{}{'}\sum_{ij} \delta_{n,i} \delta_{n,j} (\mathbf{r}_i - \mathbf{r}_j)^2.$$

Thus,

$$r_{\mathrm{rel}}^2 = r_{\mathrm{rel},pp}^2 + r_{\mathrm{rel},pn}^2 + r_{\mathrm{rel},nn}^2. \tag{A6}$$

These operators are convenient to consider in the evaluation of two-body matrix elements, since their matrix elements are simply connected to those of r_{rel}^2. The matrix elements of $r_{\mathrm{rel},pp}^2$ are obtained by restricting those of r_{rel}^2 to the proton-proton sector, $i.e.$, $\langle cd; J | r_{\mathrm{rel},pp}^2 | ab; J \rangle_{pp} = \langle cd; J | r_{\mathrm{rel}}^2 | ab; J \rangle_{pp}$, with matrix elements in other sectors vanishing. Similarly, the matrix elements of $r_{\mathrm{rel},pn}^2$ are obtained by restricting those of r_{rel}^2 to the proton-neutron sector, and the matrix elements of $r_{\mathrm{rel},nn}^2$ are obtained by restricting those of r_{rel}^2

to the neutron-neutron sector. Then, the relative square-radius operators of interest are expressed in terms of these as

$$r_p^2 = \frac{(2A - N_p)}{N_p} r_{\text{rel},pp}^2 + \frac{(A - N_p)}{N_p} r_{\text{rel},pn}^2 - r_{\text{rel},nn}^2, \tag{A7}$$

and, interchanging labels $(p \leftrightarrow n)$,

$$r_n^2 = -r_{\text{rel},pp}^2 + \frac{(A - N_n)}{N_n} r_{\text{rel},pn}^2 + \frac{(2A - N_n)}{N_n} r_{\text{rel},nn}^2. \tag{A8}$$

The equivalence of the expressions for r_p^2 and r_n^2 in (A1) to those in (A7) and (A8) may be verified in a straightforward fashion [*e.g.*, by expanding the squares in both expressions, so that the resulting expressions contain only one-body and separable two-body terms as in (A4), and comparing terms]. The relations (A7) and (A8) immediately allow the two-body matrix elements of r_p^2 and r_n^2 to be obtained in terms of those of r_{rel}^2. For instance, from the first term of (A7), we read off $\langle cd; J | r_p^2 | ab; J \rangle_{pp} = [(2A - N_p)/N_p] \langle cd; J | r_{\text{rel}}^2 | ab; J \rangle_{pp}$.

---

[1] P. Navrátil, J. P. Vary, and B. R. Barrett, Phys. Rev. Lett. **84**, 5728 (2000).

[2] P. Navrátil, J. P. Vary, and B. R. Barrett, Phys. Rev. C **62**, 054311 (2000).

[3] B. R. Barrett, P. Navrátil, and J. P. Vary, Prog. Part. Nucl. Phys. **69**, 131 (2013).

[4] C. Forssen, J. P. Vary, E. Caurier, and P. Navratil, Phys. Rev. C **77**, 024301 (2008).

[5] S. K. Bogner, R. J. Furnstahl, P. Maris, R. J. Perry, A. Schwenk, and J. Vary, Nucl. Phys. A **801**, 21 (2008).

[6] P. Maris, J. P. Vary, and A. M. Shirokov, Phys. Rev. C **79**, 014308 (2009).

[7] S. A. Coon, M. I. Avetian, M. K. G. Kruse, U. van Kolck, P. Maris, and J. P. Vary, Phys. Rev. C **86**, 054002 (2012).

[8] R. J. Furnstahl, G. Hagen, and T. Papenbrock, Phys. Rev. C **86**, 031301 (2012).

[9] S. N. More, A. Ekstrom, R. J. Furnstahl, G. Hagen, and T. Papenbrock, Phys. Rev. C **87**, 044326 (2013).

[10] E. D. Jurgenson, P. Maris, R. J. Furnstahl, P. Navratil, W. E. Ormand, and J. P. Vary, Phys. Rev. C **87**, 054312 (2013).

[11] B. Jonson, Phys. Rep. **389**, 1 (2004).

[12] I. Tanihata, H. Savajols, and R. Kanungo, Prog. Part. Nucl. Phys. **68**, 215 (2013).

[13] S. Quaglioni and P. Navrátil, Phys. Rev. C **79**, 044606 (2009).

[14] C. Cockrell, J. P. Vary, and P. Maris, Phys. Rev. C **86**, 034325 (2012).

[15] P. Maris and J. P. Vary, Int. J. Mod. Phys. E **22**, 1330016 (2013).

[16] J. Suhonen, *From Nucleons to Nucleus* (Springer-Verlag, Berlin, 2007).

[17] E. J. Weniger, J. Math. Phys. **26**, 276 (1985).

[18] H. Shull and P.-O. Löwdin, J. Chem. Phys. **23**, 1362 (1955).

[19] M. Rotenberg, Ann. Phys. (N.Y.) **19**, 262 (1962).

[20] M. Rotenberg, Adv. At. Mol. Phys. **6**, 233 (1970).

[21] S. Jacobs, M. G. Olsson, and C. Suchyta, III, Phys. Rev. D **33**, 3338 (1986).

[22] B. D. Keister and W. N. Polyzou, J. Comput. Phys. **134**, 231 (1997).

[23] M. Pervin, *Semileptonic decay of heavy baryons in a constituent quark model*, Ph.D. thesis, Florida State University (2005).

[24] E. S. R. Woodhouse and Z. Papp, Phys. Rev. C **86**, 067001 (2012).

[25] M. A. Caprio, P. Maris, and J. P. Vary, Phys. Rev. C **86**, 034312 (2012).

[26] S. Coon and M. K. G. Kruse, in *Proceedings of the International Conference Nuclear Theory in the Supercomputing Era 2013*, edited by A. M. Shirokov and A. I. Mazur (Pacific National University, Khabarovsk, Russia, 2014), p. 314.

[27] R. J. Furnstahl, S. N. More, and T. Papenbrock, Phys. Rev. C **89**, 044301 (2014).

[28] M. A. Caprio, P. Maris, and J. P. Vary, in *Proceedings of the International Conference Nuclear Theory in the Supercomputing Era 2013*, edited by A. M. Shirokov and A. I. Mazur (Pacific National University, Khabarovsk, Russia, 2014), p. 325.

[29] M. Moshinsky and Y. F. Smirnov, *The Harmonic Oscillator in Modern Physics* (Harwood Academic Publishers, Amsterdam, 1996).

[30] D. H. Gloeckner and R. D. Lawson, Phys. Lett. B **53**, 313 (1974).

[31] G. Hagen, M. Hjorth-Jensen, and N. Michel1, Phys. Rev. C **73**, 064307 (2006).

[32] Z.-T. Lu, P. Mueller, G. W. F. Drake, W. Nörtershäuser, S. C. Pieper, and Z.-C. Yan, Rev. Mod. Phys. **85**, 1383 (2013).

[33] I. Sick, Phys. Rev. C **77**, 041302(R) (2008).

[34] L.-B. Wang, P. Mueller, K. Bailey, G. W. F. Drake, J. P. Greene, D. Henderson, R. J. Holt, R. V. F. Janssens, C. L. Jiang, Z.-T. Lu, T. P. O'Connor, R. C. Pardo, K. E. Rehm, J. P. Schiffer, and X. D. Tang, Phys. Rev. Lett. **93**, 142501 (2004).

[35] P. Mueller, I. A. Sulai, A. C. C. Villari, J. A. Alcántara-Núñez, R. Alves-Condé, K. Bailey, G. W. F. Drake, M. Dubois, C. Eléon, G. Gaubert, R. J. Holt, R. V. F. Janssens, N. Lecesne, Z.-T. Lu, T. P. O'Connor, M.-G. Saint-Laurent, J.-C. Thomas, and L.-B. Wang, Phys. Rev. Lett. **99**, 252501 (2007).

[36] M. Brodeur, T. Brunner, C. Champagne, S. Ettenauer, M. J. Smith, A. Lapierre, R. Ringle, V. L. Ryjkov, S. Bacca, P. Delheij, G. W. F. Drake, D. Lunney, A. Schwenk, and J. Dilling, Phys. Rev. Lett. **108**, 052504 (2013).

[37] J. L. Friar, J. Martorell, and D. W. L. Sprung, Phys. Rev. A **56**, 4579 (1997).

[38] I. Tanihata, H. Hamagaki, O. Hashimoto, S. Nagamiya, Y. Shida, N. Yoshikawa, O. Yamakawa, K. Sugimoto, T. Kobayashi, D. E. Greiner, N. Takahashi, and Y. Nojiri, Phys. Lett. B **160**, 380 (1985).

[39] G. Alkhazov, A. Dobrovolsky, P. Egelhof, H. Geissel, H. Irnich, A. Khanzadeev, G. Korolev, A. Lobodenko, G. Mnzenberg, M. Mutterer, S. Neumaier, W. Schwab, D. Seliverstov, T. Suzuki, and A. Vorobyov, Nucl. Phys. A **712**, 269 (2002).

[40] I. Tanihata, T. Kobayashi, O. Yamakawa, S. Shimoura, K. Ekuni, K. Sugimoto, N. Takahashi, T. Shimoda, and H. Sato, Phys. Lett. B **206**, 592 (1988).

[41] I. Tanihata, D. Hirata, T. Kobayashi, S. Shirnoura, K. Sugimoto, and H. Toki, Phys. Lett. B **289**, 261 (1992).

[42] J. S. Al-Khalili, J. A. Tostevin, and I. J. Thompson, Phys. Rev. C **54**, 1843 (1996).

[43] A. M. Shirokov, J. P. Vary, A. I. Mazur, and T. A. Weber, Phys. Lett. B **644**, 33 (2007).

[44] P. Sternberg, E. G. Ng, C. Yang, P. Maris, J. P. Vary, M. Sosonkina, and H. V. Le, in *SC '08: Proceedings of the 2008 ACM/IEEE Conference on Supercomputing* (IEEE Press, Piscataway, NJ, 2008), Article No. 15.

[45] P. Maris, M. Sosonkina, J. P. Vary, E. Ng, and C. Yang, Procedia Comput. Sci. **1**, 97 (2010).

[46] H. M. Aktulga, C. Yang, E. G. Ng, P. Maris, and J. P. Vary, Concurrency Computat.: Pract. Exper. (2013), DOI: 10.1002/cpe.3129.

[47] A. M. Shirokov, V. A. Kulikov, P. Maris, and J. P. Vary, in *NN and 3N Interactions*, edited by L. D. Blokhintsev and I. I. Strakovsky (Nova Science, Hauppauge, N.Y., 2014), Chap. 8.

[48] Ch. Constantinou *et al.* (in preparation).

[49] R. J. Furnstahl, G. Hagen, T. Papenbrock, and K. A. Wendt, J. Phys. G (submitted), `arXiv: 1203.2515`.

[50] G. A. Negoita, *Ab initio nuclear structure theory*, Ph.D. thesis, Iowa State University (2010).

[51] G. A. Negoita *et al.* (in preparation).

[52] S. Bacca, N. Barnea, and A. Schwenk, Phys. Rev. C **86**, 034321 (2012).

[53] S. Quaglioni, C. Romero-Redondo, and P. Navrátil, Phys. Rev. C **88**, 034320 (2013).

[54] T. Helgaker, P. Jørgensen, and J. Olsen, *Molecular Electron-Structure Theory* (Wiley, Chichester, 2000).